Microstructural Analysis of Tristructural Isotropic Particles in High-Temperature Steam Mixed Gas Atmospheres*

Katherine I. Montoya[a,†], Brian A. Brigham[a], Grant Helmreich[b], Jesse Werden[b], Tyler J. Gerczak[b], and Elizabeth S. Sooby[a]

[a] Department of Physics and Astronomy, University of Texas at San Antonio, San Antonio, TX, 78249, USA
[b] Reactor and Nuclear Systems Division, Oak Ridge National Laboratory, Oak Ridge, TN, 37831, USA

Abstract

High-temperature gas-cooled reactors (HTGRs) use tristructural isotropic (TRISO) particles embedded in a graphitic matrix material to form the integral fuel element. Potential off-normal reactor conditions for HTGRs include steam ingress with temperatures above 1,000°C. Fuel element exposure to steam can cause the graphitic matrix material to evolve, forming an atmosphere composed of oxidants and oxidation products and potentially exposing the TRISO particles to these conditions. Investigating the oxidation response of TRISO particles exposed to a mixed gas atmosphere will provide insight into the stability under off-normal conditions. In this study, surrogate TRISO particles were exposed to high temperatures (T = 1,200°C) in flowing steam (5% < pH$_2$O < 21%) and CO (pCO < 1%) to determine the oxidation behavior of the SiC layer when exposed to various mixed gas atmospheres. Scanning electron microscopy, x-ray diffraction, and focused ion beam milling was used to determine the impact of CO and steam on the oxidation behavior of the SiC layer. The data presented demonstrates how the SiC layer showed strong oxidation resistance due to limited SiO_2 growth and maintained its structural integrity under these off-normal conditions.

Highlights

Steam oxidation results of SiC at 1,200°C in 5–21% steam and 0–1% CO
SiO_2 growth were measured in low partial pressure of steam with CO present
Crystalline SiO_2 formed under all conditions
SiC layer displays microstructural degradation in a high-temperature mixed gas atmosphere

Keywords

High-temperature gas reactor
Silicon carbide
Steam oxidation
Ion milling techniques
Nuclear fuel
TRISO

† Corresponding author: *E-mail address:* katherine.montoya@utsa.edu (K.I. Montoya).

Microstructural Analysis of Tristructural Isotropic Particles in High-Temperature Steam Mixed Gas Atmospheres

1.Introduction

Tristructural isotropic (TRISO) particles are the proposed fuel form for high-temperature gas-cooled reactors (HTGRs) [1, 2]. The TRISO design features four coating layers (three graphitic and one silicon carbide (SiC)) that surround the actinide-bearing fuel kernel and provide structural stability and fission product retention. The TRISO particles are typically encapsulated in a graphitic matrix material composed of graphite flake and carbonized resin to form fuel elements (e.g., cylindrical compacts or spherical pebbles). Multiple failure mechanisms of TRISO particles have been identified, some of which can lead to the cracking of the SiC layer [3]. Nuclear fuel performance codes such as PARFUME and BISON have been used to assess different SiC layer failures but have yet to model all the phenomena [4-6]. Thinning of the SiC layer increases the probability of SiC failure, specifically cracking and/or rupture, due to a reduction of structural material to withstand internal particle pressure caused by fission gas and/or carbon monoxide (CO) production. Appreciable CO build-up and SiC deterioration caused by a chemical attack by CO is seen explicitly in UO_2 kernels at high burnups but is not as prevalent in the UCO TRISO kernels. Thinning of SiC can occur in localized areas due to buffer and inner pyrolytic carbon (IPyC) fracture. Under more extreme irradiation conditions and temperatures (T>1,800°C), IPyC cracking can occur. The compromised IPyC layer can provide an additional pathway for fission products, such as palladium, to accumulate, corrode, and degrade the SiC layer. This fission product interaction causes localized thinning of the SiC layer and increases stress on the region resulting in a higher probability of SiC failure. This mechanism of a failed IPyC layer and compromised SiC layer due to fission product interactions was found to only occurred in only a few UCO particles [7-9]. Both modeling efforts and experimental results determined that the structural strength of the SiC layer in the traditional TRISO designs decreases as it thins [4-6, 10]. The SiC layer will still be able to withstand typical HTGR operating conditions until it reaches the critical point of 20 μm [4-6, 11].

For an HTGR utilizing a Rankine power cycle, a hypothesized off-normal reactor condition would be produced in the core if the secondary cooling line were to rupture, causing the helium coolant to become contaminated with the secondary coolant [12, 13]. In designs where the secondary heat transfer medium is steam, the depressurized loss of forced cooling could result in steam exposure to fuel elements. Depending on the temperature and partial pressures of oxidant ingress, some matrix material will volatilize, producing a mixed-gas atmosphere that contains both steam and volatile graphite oxidation products [14]. If sufficient oxidation occurs, the fuel element's structural integrity, specifically the SiC layer, may be degraded [14].

Under HTGR accident conditions, the steam partial pressure can reach 400 kPa pH_2O, but lower partial pressures <3 kPa pH_2O are more likely and can vary by reactor design [12, 13, 15-17]. Brigham *et al.* demonstrated that the exposure of matrix material to steam reduces the partial pressures of oxidants (as H_2O and O_2 are consumed) and produces significant concentrations of CO, CO_2, and H_2 at T>800°C [18]. At high temperatures (T>800°C) and lower partial pressures of steam (<10 kPa pH_2O), the reported CO mass spectrometry signal was greater than CO_2, indicating CO is the predominant graphite matrix oxidation product in simulated HTGR accidents involving lower, less than 10%, partial pressures of steam [18]. Oxidation of the SiC layer by either chronic or acute exposure to oxidants in the He coolant would lead to SiC layer recession and the

subsequent growth of SiO_2 (i.e., passive oxidation) or volatilization of silicon hydroxides (i.e., active oxidation). During high-temperature steam exposure, the passive oxidation behavior of SiC can be described by the formation of a protective silica (SiO_2) scale that slows the transport of oxygen to the bulk SiC material.

Thermodynamically, SiC reaction with steam and CO is anticipated to be governed by Equations 1 and 2 due to the more negative change in Gibbs Free Energy (ΔG) per mole reactant. The ΔG is presented for equations 1–5 at 1,200°C as calculated using the 'Reaction Equations' module in HSC chemistry [19]. Equation 1 is considered the global steam reaction equation that describes the often passivating behavior that has been reported up to 1,200°C in $H_2O_{(g)}$. Equation 3 is the primary active, volatile forming response for SiC that may occur in the active regime [20-22]. Equation 4 describes the reaction where the oxidation potential in this atmosphere can be reduced and potentially limit the amount of oxide growth due to $CO_{(g)}$. Equations 3,5, and 6 are potential reactions that can occur if the oxidation regime is active would result in some loss of the SiO_2 layer or prevent further growth .

ΔG= -518.125 kJ	$SiC_{(s)} + 3H_2O_{(g)} = SiO_{2\,(s)} + 3H_{2\,(g)} + CO_{(g)}$	(1)
ΔG= -333.109 kJ	$SiC_{(s)} + 2CO_{(g)} = SiO_{2(s)} + 3C_{(s)}$	(2)
ΔG= -73.410 kJ	$SiC_{(s)} + CO_{(g)} = SiO_{(g)} + 2C_{(s)}$	(3)
ΔG= -28.415 kJ	$CO_{(g)} + H_2O_{(g)} = CO_{2\,(g)} + H_{2\,(g)}$	(4)

As SiO_2 grows in thickness, the oxidizing reaction described by Equation 6 can occur simultaneously and eventually reach a steady-state thickness where the SiO_2 volatilizes as a hydroxide at the same rate that the oxide forms. This dynamic is often observed as a para-linear oxidation response [23]. Although Equation 5 is less thermodynamically favorable due to its positive ΔG value, experimentally, it has been seen that the SiO_2 can be formed and then reduced, leading to volatilization of the oxide if the partial pressure of CO is sufficient. Increasing the local partial pressure of CO can prevent further formation of the SiO_2 layer and potentially damage the layer [24]. If active oxidation occurs after the formation of the SiO_2, the volatilization of SiO_2 (cristobalite) can follow Equations 6 with $Si(OH)_{4(g)}$ as the primary volatile reaction product as observed in high-temperature steam experiments [20, 22]. Equation 6 dominates for high partial pressures of steam and high temperatures as the SiC undergoes active oxidation [20]. The predominance of $Si(OH)_{4(g)}$ is dependent on the pH_2O and temperature and has been experimentally measured to produce a small amount (~10^{-5} bar) at 1,300°C in 1 atm steam [20, 22, 25]. The ΔG seen in Equation 6 further suggests that this reaction is thermodynamically unfavorable at temperatures below 1,200°C and pressures below 10^{-7} MPa, however the phenomena is observed in numerous studies [20, 22, 26] at T≥1,200°C, potentially progressing in a multistep reaction.

ΔG= 266.355 kJ	$SiO_{2\,(s)} + CO_{(g)} = SiO_{(g)} + CO_{2\,(g)}$	(5)
ΔG= 153.915 kJ [22]	$SiO_{2\,(s)} + 2H_2O_{(g)} = Si(OH)_{4\,(g)}$	(6)

Bulk SiC oxidation behavior has also been studied by Opila *et al*. [27-29] in combustion environments and reducing mixed gas atmospheres where H_2O, O_2, CO, and CO_2 are present. Although the concentrations of the gases presented are not representative of a reactor scenario, the

studies provide insight into the oxidation response of SiC to mixed gases. Opila *et al*. determined that atmospheres composed of both oxidizing and reducing gases (CO_2 and CO) can inhibit the growth of the passive SiO_2 layer by reducing the pO_2 in the atmosphere, preventing further SiO_2 growth and can lead to volatilization of the SiO_2 [21]. Additionally, Opila *et al.* determined that in atmospheres composed of CO-CO_2 and H_2O-H_2 mixtures, where both oxidizing and reducing agents are present, the partial pressure of the oxidant (CO_2 and H_2O in that study) allows for the formation of the SiO_2, it is not able to prevent the volatilization of the SiO_2 layer [28, 30, 31]. The presence of the reducing agent consumes any free oxygen present in the atmosphere and contributes to mass loss due to the interaction with the reducing agents and the SiO_2.

Exploring the impact of an HTGR accident-relevant steam and CO mixed gas atmospheres provides insight into the microstructural response of the SiC layer to oxidation. Exposure of the SiC layer to an oxidizing, mixed gas atmosphere could compromise the SiC. Some fission products are present in the SiC layers after irradiation of TRISO fuel [32, 33]. Oxidation SiC layer may lead to thinning of the SiC layer leading to increase probability of fuel failure [5, 6]. The investigation presented here includes particle exposure to steam and relevant CO concentrations (0.1 and 1% mol fraction) to simulate mixed gas atmospheres after matrix graphite oxidation. These conditions model the off-normal scenario of the contaminated coolant introducing oxidants to the TRISO particles after the matrix and outer PyC (OPyC) layer have evolved and exposed the SiC layer. The objective of this study is to probe partial pressures of steam and CO. Determining the behavior of the SiC layer using microstructural characterization and x-ray diffraction (XRD) to understand the microstructural and thermochemical degradation of TRISO particles when exposed to high-temperature mixed gas atmospheres.

2. Materials and Methods

2.1 Materials

Oxidation testing and microstructural characterization were conducted on AGRBW-4A2 ZrO_2 kernel particles, which are ~0.6 mm in diameter and weigh ~0.7 mg each, received from Oak Ridge National Laboratory (Oak Ridge, Tennessee, USA). These surrogate coated particles, referred to as SiC-terminated, were fabricated without the buffer layer or outer pyrolytic carbon (OPyC) layer specifically for systematic strength testing of fluidized bed chemical vapor deposition (FBCVD). The resulting SiC layer is the outermost layer in this particular particle design and maintains relevant features to TRISO fuel architectures [34, 35]. The exposed SiC layer produced a SiC layer with near-representative properties to those found in typical TRISO fuel, while the exposed SiC outer surface allows for direct observation of the oxidation response of the SiC layer in the absence of the OPyC layer.

2.2 TRISO oxidation testing

The SiC-terminated particles were subjected to oxidation testing in a Netzsch F3 449 Jupiter Simultaneous Thermal Analyzer (STA) (449 F3, Netzsch Instruments, Selb, Germany) equipped with a SiC element furnace with a water vapor adapter (1,600°C maximum temperature) and inline RapidOx O_2 sensors (RapidOx OEM447, Cambridge Sensotec) to measure trace, contaminant O_2 levels. During each test, 200 particles were placed in an additively manufactured yttria-stabilized zirconia (YSZ) mesh basket in a hanging sample configuration. The custom basket design is

intended to allow for laminar flow of gas over and around the particles while limiting the potential of fixturing interaction within the furnace. During the thermal ramp, argon (Ar) was purged through the furnace at 200 standard cubic centimeters per minute (sscm) via the integrated STA mass flow controllers and 8 NL/hr (112 sscm) via the heated stainless-steel water vapor generator transfer line, as the system was heated at 10°C/min to the isothermal test temperature. To allow the system to thermally equilibrate, the system was held at 1,200°C under an Ar-only atmosphere for 20 minutes before steam and CO were introduced for the 10-hr isotherm. The system was cooled to room temperature at 20°C/min with flowing Ar. Steam generation rates were 0.75, 2, and 4.0 g/hr to target corresponding mole fractions of 5, 9, and 21% steam. While CO from either a 0.1% or 2% secondary standard gas cylinder (balance Ar) was injected into the furnace at 100 sscm for corresponding concentrations of 1,000 and 10,000 ppm, respectively. Steam generation rates remained the same as CO was introduced at either 0.1% or 1%. The unchanged steam rates allowed for the total moles of steam exposed to the sample to remain the same for each subset of tests (.75, 2 and 6 g/hr), though the overal partial pressure is reduced due to the dilution of the steam with CO and the Ar carrier gas, as per Dalton's law. The steam-only conditions allow for comparison to the respective steam with CO-exposed specimens in the condition set to determine the impact of high-temperature CO and steam on the microstructure. The naming scheme labels the conditions as steam-only, 0.1%, and 1% CO as conditions of the steam flow conditions. The exposures were performed at T=1,200°C for 10-hour isotherms with varying partial pressures of steam (5% < pH$_2$O < 21%) and CO (0.1% and 1.0%) as summarized in Table 1. The mixture concentrations for each exposure were calculated via the Ar/CO calibration factor, Ar purge flow rate, and water mass flow rate. The measured change in mass was within the error of the TGA measurement technique, and thus the TG results are not presented here. Specifically, the mass change over the course of the 10-hour exposure is comparable to drift in baseline measurements. The lack of quantifiable weight change demonstrates, despite the sample size containing 200 particles, there is difficulty in determining the amount of oxide grown during exposures due to the slow kinetics of SiC oxidation. Any slight changes are within the error of the measurement technique.

ID	Carrier Gas flow rate (NL/h)	Purge gas rate (sscm)	Water mass flow (g/h)	Resulting Condition
1	8	200	4.0	21% H_2O
2	8	200	4.0	21% H_2O + 0.1% CO
3	8	200	4.0	21% H_2O + 1% CO
4	8	200	1.5	9% H_2O
5	8	200	1.5	9% H_2O + 0.1% CO
6	8	200	1.5	9% H_2O + 1% CO
7	8	200	0.75	5% H_2O
8	8	200	0.75	5 H_2O % + + 0.1% CO
9	8	200	0.75	5% H_2O +1% CO

Table 1-Summary of exposure conditions of 10-hr at 1200°C isotherms with varying pH$_2$O and pCO.

2.3 X-ray diffraction

A Bruker D2 phaser benchtop powder x-ray diffractometer was used to collect diffraction patterns of the particles pre-and post-exposure to compare the crystallographic phase compositions. The 200 particles pre-and post-exposure were placed in a low background holder with measurements taken from 18 to 80° 2θ with a 0.01 step size and 3-second dwell time per step. Surveying whole particles provides a non-destructive method for acquiring data on the crystallographic phases and allows for SEM characterization of the same as-oxidized TRISO particles following oxidation exposure. Data processing and visualization were performed on Bruker DiffracEVA (version 5.0) software. To determine the phase abundance for each exposure, each phase was normalized to its corresponding powder diffraction file (PDF), and then the semi-quantitative analysis function on the DiffracEVA software was used to quantify the relative phase abundance. The semi-quantitative technique uses the normalized intensity of the main peak from the reference PDF and fits it to the main peak of the obtained spectra to determine the relative abundance for each phase. The semi-quantitative analysis can result in some uncertainty in the measured amount of each phase because the main peak can be significantly more intense than the others, leading to an over- or underestimation of the other peaks causing the relative abundance of this phase not to be accounted for fully. This measurement was intended to provide an estimated ratio of the SiC and SiO_2 phase abundances and identify any trends. Each set of conditions had a consistent C amount suggesting that the phase values could provide a relative ratio.

2.4 Scanning electron microscopy

Top-down scanning electron microscopy (SEM) was used to visualize the evolved microstructure of the SiC surface pre-and post-exposure. TRISO particles were cleaned before imaging by using an ultrasonic bath (acetone followed by methanol) to eliminate debris from the particles' surface. SEM analysis was performed on a Hitachi FlexSEM 1000 equipped with secondary electron (SE) and backscatter electron (BSE) detectors. BSE images were used to identify surface structures and potential compositional changes in the structure. Ten particles were selected from each condition to observe the microstructural evolution of the surface of the SiC layer. Top-down or as-oxidized imaging targeted the observation of the change in surface morphology of the SiC surface and SiO_2 formation. Initial SEM characterization, as shown in Figure 1, displays the as-received particle surface. The rough surface results from the termination of the columnar SiC grains during the fluidized bed chemical vapor deposition fabrication process [36].

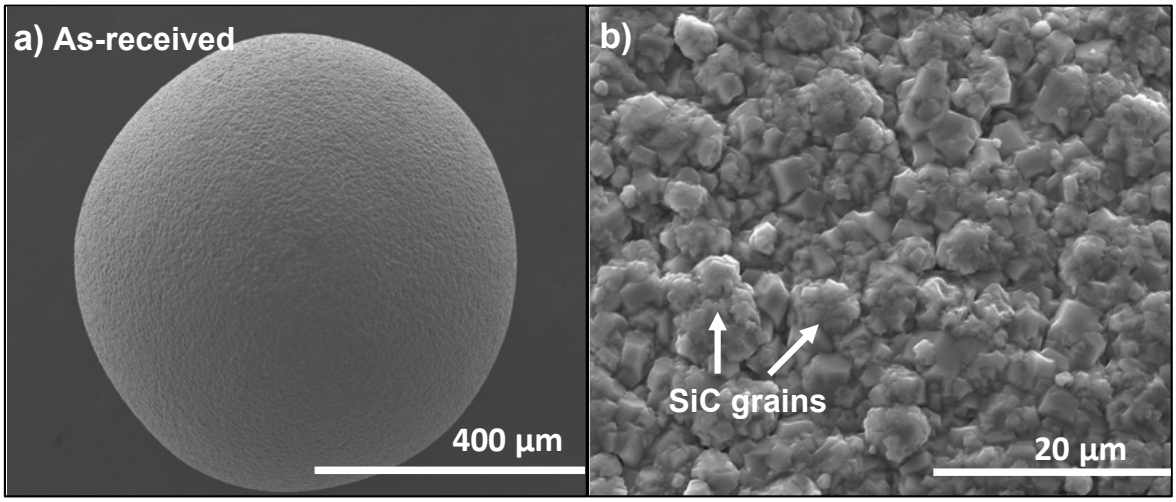

Figure 1. BSE micrographs of as-received TRISO SiC-terminated particles with (a) the SiC layer as the outermost layer and (b) the initial uneven SiC surface.

Focus ion beam (FIB) milling was performed on an FEI Versa dual-beam FIB-SEM equipped with a Ga^+ focused ion beam to analyze the SiO_2-SiC interface and measure oxide growth. In a previous study [37], FIB milling on uncross-sectioned TRISO particles was successfully demonstrated for an oxide thickness analysis on SiC by trenching. The cross-sections provide information on oxide thickness, pore formation, and SiO_2 layer cracking. Cross-section images of the oxide layer were acquired in SE mode at 5 keV in high-vacuum mode. Pt was deposited on the surface to prevent rounding and accurately measurement of the SiO_2 thickness. FIB milling was performed on two particles for each exposure with two milled locations on the selected particles. ImageJ (1.8.0_172) was used to determine the thickness of the SiO_2 layer using an average of twenty measurements for each exposure condition [38]. This method was performed for all oxidized particles for both locations on each particle. The brightness and contrast of the micrographs were adjusted to create a distinction between SiO_2-SiC and Pt-SiO_2 interfaces, and then SiO_2 thickness measurements were made. Two select whole particles were cross-sectioned using a Hitachi ArBlade 5000 ion milling system, as shown in Figure 2, and imaged using the Hitachi FlexSEM 1000. This method complements and validates thickness measurements from FIB prepared samples.

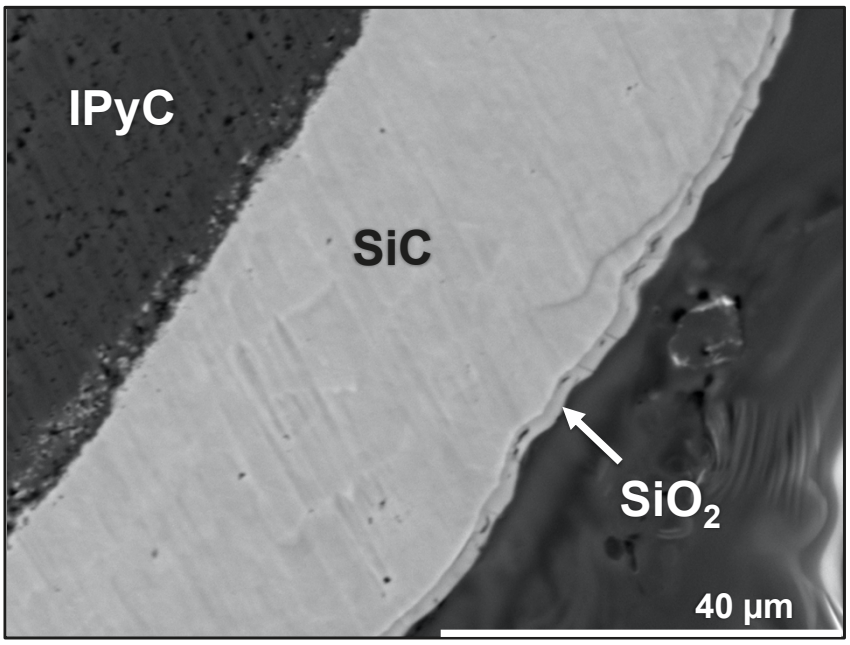

Figure 2-Surface ion milled cross-section of SiC-terminated particle exposed to 1,200°C, 21% steam with preserved SiO_2-SiC interface

2.5 Optical Microscopy

Optical microscopy was performed using Olympus DSX500 Opto-Digital Microscope equipped with a 10X lens. Micrographs were used to measure diameters of as-received and oxidized particles using shadow imaging [39]. Images were calibrated using 1 mm ball bearings to determine the image resolution. The stitching feature in the Olympus software allowed for imaging of a larger area to prevent repeated measurements of the particles. Combining the diameter results obtained during shadow imaging with the reported kernel and IPyC dimensions as well as the SiO_2 thickness measurements provides insight into potential changes in the SiC layer.

3. Results

3.1 X-ray diffraction analysis

The XRD data obtained after each exposure are arranged by increasing pH_2O and pCO atmosphere in Figure 3. The powder diffraction files (PDFs) of each identified phase are also listed in Figure 3. Targeted phases included SiC, SiO_2, C (graphite), and ZrO_2. A shift of -0.122° 2θ was observed and fit to the main SiC peak at 35.6° for all measurements. The observed shift is due to the height difference of the particles with respect to the standardized measurement plane. The as-received spectrum of the particles displayed notable peaks for SiC, C (IPyC), and ZrO_2, which correspond to the fabricated layers with no SiO_2 detected. Identified C phase is within the approximate 40 µm probing depth of the XRD. The ZrO_2 phase may be due to kernel contributions. The intensity of the SiC peaks is mainly unaffected by the exposures.

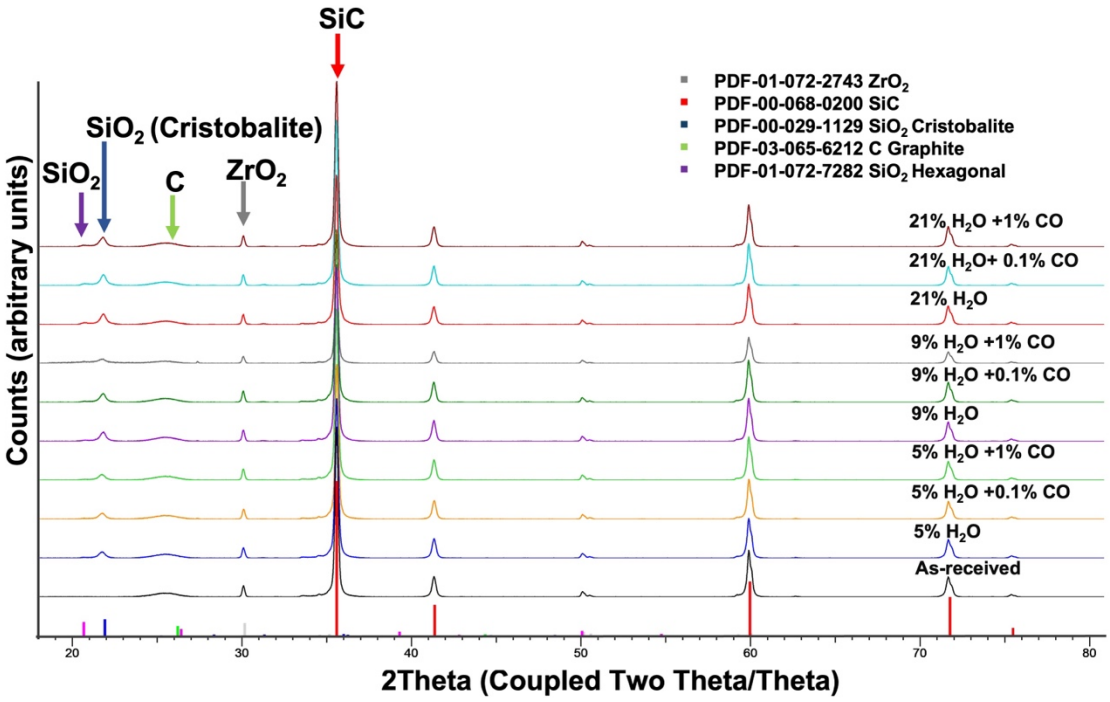

Figure 3. XRD patterns of as-received and as-oxidized TRISO particles samples are arranged by increasing steam exposure. The main peaks of each identified phase are denoted with an arrow corresponding to a PDF color.

Semiquantitative analysis was performed in the DiffracEva (version 5.0) software for each XRD scan, and the results are presented in Table 2. XRD analysis confirmed the presence of SiO_2 and determined that cristobalite with a minor, secondary hexagonal SiO_2 phase formed for all conditions. The semiquantitative analysis focused on the ratio of SiC consumption to the formation of SiO_2. The ZrO_2 and C abundances were nearly identical for all scans because these contributions are from the surrogate kernel and IPyC layer which should be unaffected by the exposure. Any changes in the C phase can be attributed to the varying SiC-SiO_2 thickness. XRD analysis confirmed the presence of a stable crystalline SiO_2 layer under these conditions and of the SiO_2 phases that were identified, cristobalite being the dominant of the two and the greatest amount of the hexagonal phase seen in the steam-only conditions. Similarly cristobalite and quartz phases were observed in a previous high temperature steam exposure study performed on SiC exposed TRISO [40]. The SiC concentration observed here decreased as the two identified SiO_2 phase concentrations increased as shown in Table 2. The exposures containing a higher concentration of CO reduced the amount of SiO_2 formed compared to the pure steam exposures. Amorphous SiO_2 could not be detected this measurement.

	SEM Measurement	XRD Measurement				
Condition	**Average SiO_2 thickness (µm)**	**SiC**	**SiO_2 (cristobalite)**	**SiO_2 (hexagonal)**	**ZrO_2**	**C (graphite)**
As-received	-	98.7%	0.00%	0.10%	0.60%	0.60%
5% H_2O +1% CO	0.72 (SD=0.08)	97.7%	0.60%	0.60%	0.60%	0.60%
5% H_2O +0.1% CO	0.80 (SD=0.15)	97.6%	0.60%	0.60%	0.60%	0.60%
5% H_2O	0.87 (SD=0.13)	96.9%	0.60%	0.40%	0.60%	0.60%
9% H_2O +1% CO	0.95 (SD=0.12)	96.6%	0.70%	1.60%	0.60%	0.50%
9% H_2O +0.1% CO	1.04 (SD=0.10)	97.4%	0.90%	0.60%	0.60%	0.50%
9% H_2O	1.10 (SD=0.12)	97.2%	0.90%	0.70%	0.60%	0.60%
21% H_2O +1% CO	1.49 (SD=0.11)	97.2%	1.00%	0.70%	0.60%	0.50%
21% H_2O+ 0.1% CO	1.70 (SD=0.10)	96.7%	1.10%	1.10%	0.60%	0.50%
21% H_2O	1.68 (SD=0.16)	96.5%	1.20%	1.20%	0.60%	0.50%

Table 2-Summary of semi-quantitative analysis arranged by increasing pH_2O atmosphere with microscopic measurements with its standard deviation of the SiO_2 layer thickness.

3.2 Scanning Electron Microscopy Results

Figure 4 provides representative images of the particle's surface morphology post-exposure for each oxidation condition tested. All exposures displayed varying amounts of SiO_2 growth verifying the detection of SiO_2 from the XRD analysis. For the 21% steam-only exposure, the micrograph displays the most uniform oxide scale with surface cracking present. The surface cracking likely formed on cooling with the phase transition of the crystalline SiO_2 due to a mismatch in the coefficient of thermal expansion (CTE) with the base SiC layer [41-43]. The SiO_2 scale formed with the highest steam partial pressures had very little of the original surface morphology (refer to Figure 2) remaining as seen in the 21% steam column of Figure 4. The least amount of observable surface oxide present was present at the highest concentration of CO with the lowest partial pressure of steam being 5%. At 5% steam with 1% CO, there is little SiO_2 layer growth relative to other conditions, and most of the original SiC surface morphology is visible. As the CO concentration increased, it was inferred that the SiO_2 layer that formed was a non-uniform due to the as-oxidized SiC exposed surface having a similar morphology to the as-received surface of the TRISO particles seen in Figure 1. Under these conditions, the microstructure evolution may follow Eq. 3 and 5, where CO can inhibit the amount of SiO_2 formed and/or cause SiO_2 to volatilize by reducing the pH_2O as seen in Eq. 6. Volatilization would need to be confirmed via recession measurements and/or significant changes in the thermogravimetric data, which were not observed in this study. Additionally, the lower pH_2O with increased CO amount can allow for the CO amount to getter any addition H_2O, as seen in Eq. 4, further limiting the SiO_2 growth. A minimal amount of surface porosity in the SiO_2 layer was observed for all conditions.

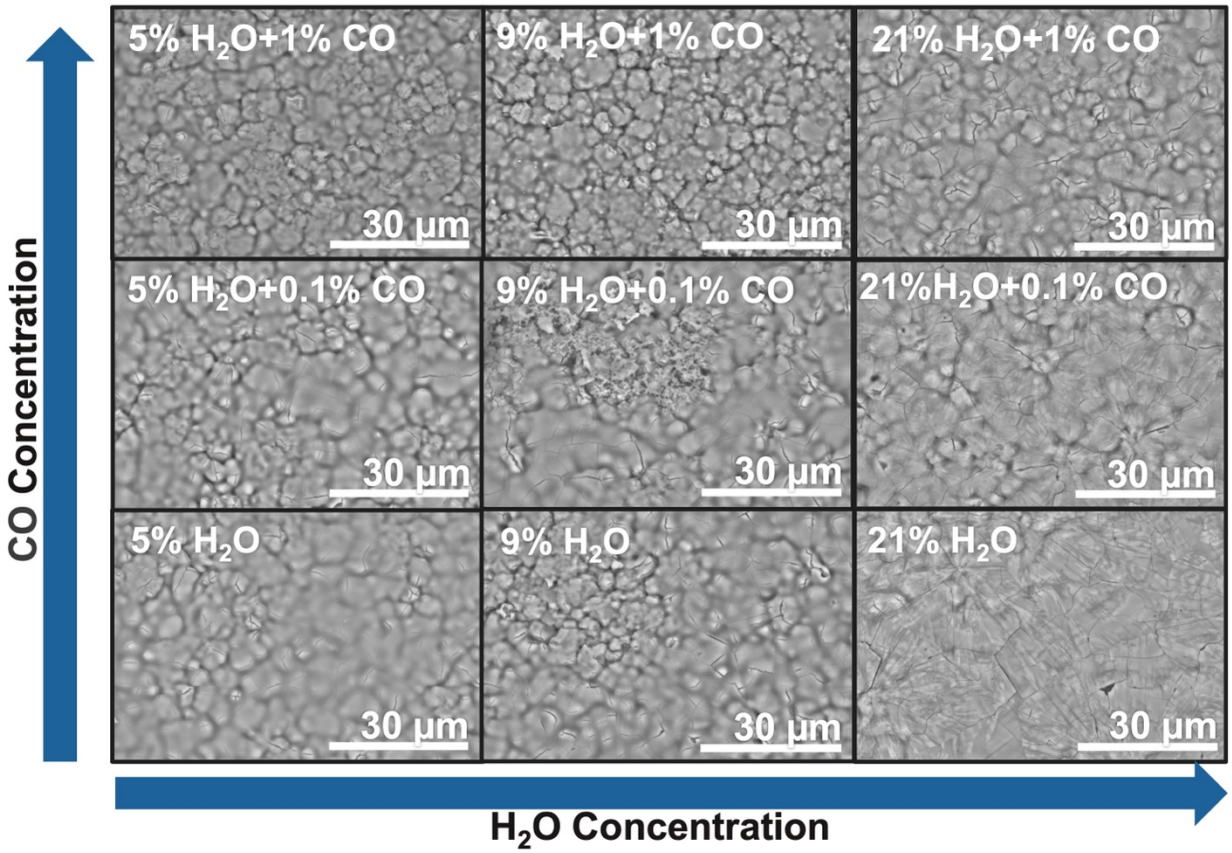

Figure 4-BSE micrographs of the evolved surface microstructures arranged by *p*H2O and *p*CO atmospheres.

In Figure 5, the surface of an oxidized TRISO particle with a selected trenching area displays the varying surface topography of the particle. The uneven surface is a function of the FBCVD deposition process and provides a rough surface for the SiO_2 to form. Figure 5 labels the topography with peaks (white arrows) and valleys (red arrow). These height differences in the SiC grains contribute to how the SiO_2 will grow from an uneven surface.

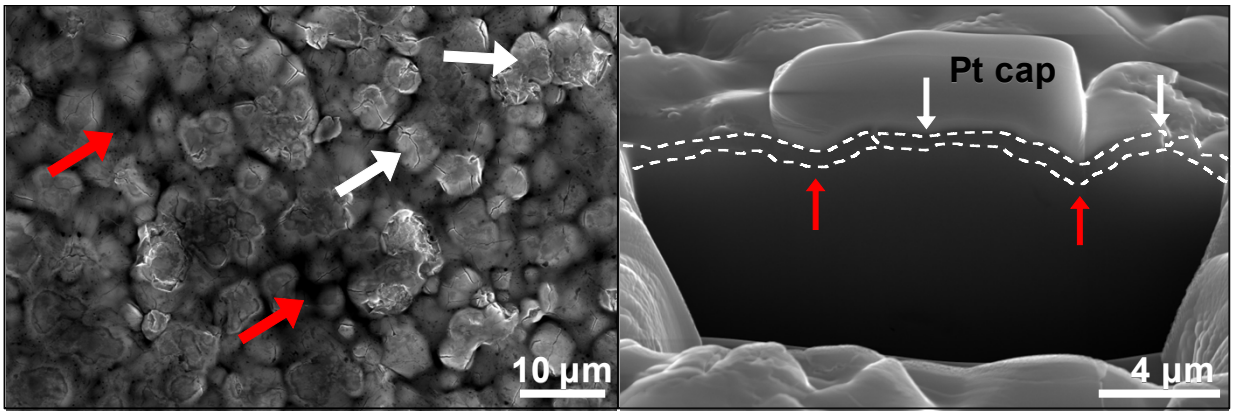

Figure 5-SE micrographs of the microstructures formed when exposed to 5% steam with 1% CO. The surface displays varying surface topographies. White arrows indicate areas of higher height differences and red arrows indicate areas of lower height difference.

Figure 6 provides representative FIB cross-sections used to determine the values shown in Table 2 arranged by the increasing steam and CO concentrations. From Figure 6, the FIB cross-sections determined that all conditions had produced a SiO_2 layer, confirming the XRD results from Section 3.1. The 21% H_2O atmospheres displayed the most oxide growth overall. The variance in oxide thickness is largest with 1% CO exposures. Conditions that contained 1% CO had lower amounts of oxide growth when compared to the steam-only conditions, suggesting that CO may inhibit the amount of SiO_2 that can form. The measured SiO_2 thickness for all exposures is <2 µm which is lower than the thicknesses reported for 100% steam exposures at similar temperatures [11, 40]. The resulting SiO_2 layer was dense with some porosity, seen in the void structures in the SiO_2 layer. The void features observed more often in the higher partial pressures of steam (pH_2O=21%) are likely due to trapped gases such as CO or H_2 produced during SiC consumption [40]. Larger pores were observed in the 1% CO conditions giving the appearance that a more complex SiO_2 layer had formed. The porosity may be attributed to the formation of H_2 shown in Eq.1 [40]. For all conditions, there is variation in the thickness of the SiO_2 as it formed on uneven SiC grains as seen in Figure 6. Vertical cracking observed in the SiO_2 layer was reported to form during cooling due to the mismatched thermal expansion coefficients of the SiO_2 and the SiC [11, 40] which was noted in the surface morphology analysis (Figure 4). XRD, surface microscopy, and FIB cross-sections provide insight into the SiO_2 presence and abundance following the mixed atmosphere exposures. However, recession cannot be quantitively determined as the overall change in particle diameter is within the diameter variation from particle to particle.

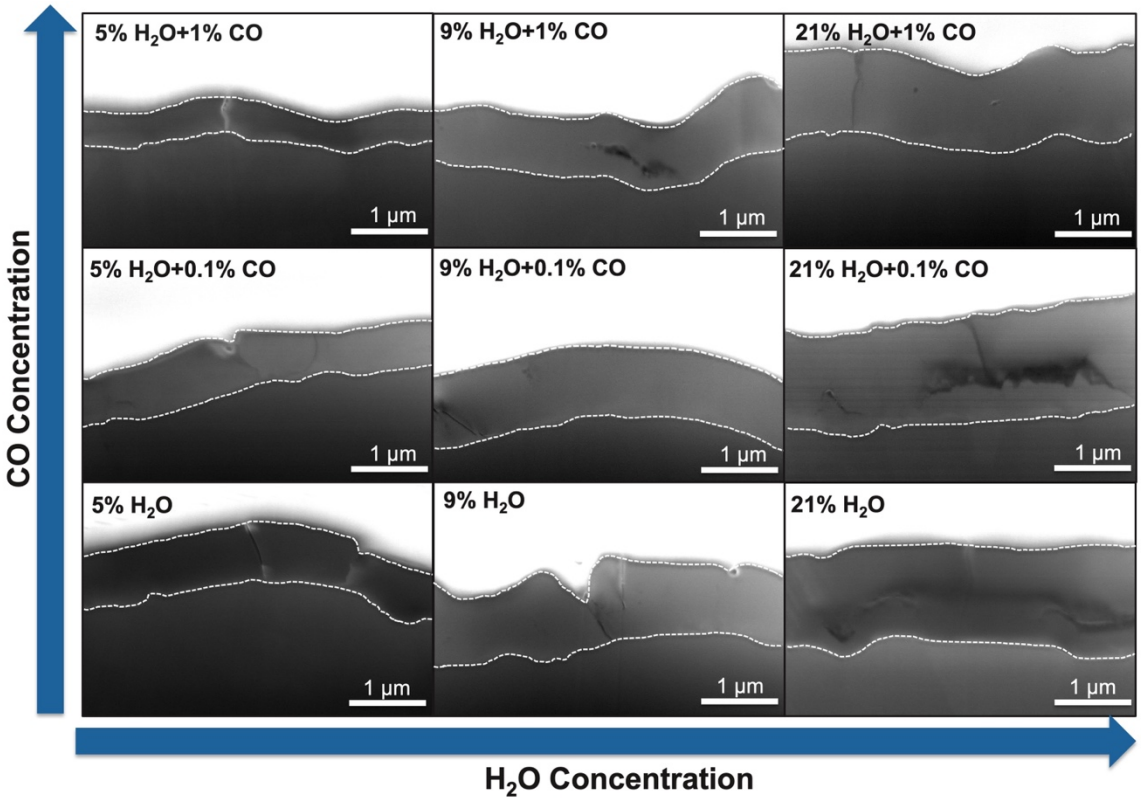

Figure 6-SE micrographs of SiO_2-SiC interface. The protective Pt layer is observed in the lightest phase, and the SiC is observed in the darkest phase. Dotted lines highlight the SiO_2 layer.

4. Discussion

4.1. Oxidation of SiC in mixed gases

SiC oxidation in the TRISO design was previously studied at high temperatures (T>1,200°C) paired with high partial pressures of steam (pH_2O>20%) [11, 40, 44]. However, low partial pressures of steam and CO as a mixed oxidant atmosphere have not been comprehensively investigated. The typical oxidation behavior seen under high partial pressures of steam conditions involves the formation of SiO_2 and its subsequent volatilization in appreciable steam concentrations at T>1,200°C. The behavior of the SiC in this investigation, when exposed to low partial pressures of the contaminants, provided insight into the oxidation mechanisms under mixed gas atmosphere composed of a oxidizing and reducing gas. The predominant behavior suggested that the SiC underwent passive oxidation to form SiO_2. Kinetic rates could not to be calculated in this study as each particle weighs ~0.7 mg, and weight changes were not distinguishable in the TG signal, even with 200 particles in each exposure. The lack of measurable weight change led to a focus on the evolution of the microstructure in the SiC layer caused by presence of high-temperature mixed gases. Oxidation testing of bulk SiC at high temperatures and high partial pressures of H_2O resulted in the formation of a SiO_2 layer. Cristobalite is the more thermodynamically favorable and stable of the two SiO_2 phases formed in this study and under high-temperature steam atmospheres (T >1,000°C) [27, 40]. Despite the presence of CO, the formation of crystalline SiO_2 was seen under all conditions. If the amount of CO is not appreciable, it cannot suppress the volatilization of the SiO_2 to $SiO_{(g)}$ due to the higher partial pressure of H_2O

[21]. The microstructures shown in this study, specifically porosity and cracking on the surface of the SiO_2 layer, have been seen in other high-temperature steam exposures [11, 40, 44, 45]. The high-temperature steam-only studies [11, 40, 44] noted pore formation in the SiO_2 layer due to diffusion and entrapment of CO and H_2 gas produced from Eq. 1. The porosity was greatest in the higher pH_2O conditions, potentially leading to a thicker oxide layer. Cracking of the SiO_2 layer upon cooling is due to differing coefficients of thermal expansion between the SiO_2 and SiC [11, 40, 44, 46]. Due to the high partial pressure of steam, the dominant oxidation mechanism observed in these studies was the formation of the SiO_2 scale. However, the SiO_2 may have reacted with the steam and formed silicon hydroxide $Si(OH)_{4\,(g)}$, which can become volatile at temperatures greater than 1,200°C, or the presence of a reducing gas may have slowed the growth of the SiO_2 layer [23].

Parabolic rate constants from Cho *et al.* and Cao *et al.* [11, 44], where comparable pH_2O at 1,200°C were tested on TRISO particles, were used to determine if the amount of oxide formed in the presented work followed a similar growth trend as seen in the two listed investigations. The amount of SiO_2 growth seen for the 5, 9, and 21% steam-only conditions were within or below the calculated value of 1.9 μm, which was extrapolated from Cho *et al.* and Cao *et al.* [11, 44]. The hypothesis was that introducing varying pCO amounts would produce thinner oxide layers than in the H_2O-only atmosphere. The 1% CO conditions favored Eq. 4, limiting the amount of oxide growth, making Eq. 1 less favorable but still the dominant reaction [21]. The differences between the extrapolated value using the rate constants from Cho *et al.* and Cao *et al.* [11, 44] and the measured SiO_2 growth in a pure H_2O atmosphere could be due to the oxidation testing method where tube furnaces equipped with alumina working tubes and fixturing were used [11, 44] versus a yttria-stabilized zirconia (YSZ) basket used in this investigation. Alumina can volatilize in high-temperature steam environments and within the tube itself can affect the oxide growth [47]. In an effort to mitigate any sample interactions with the alumina tube of the STA that could alter the oxidation rates, the particles were placed in a hanging perforated YSZ basket. Additionally, mechanical testing has been performed on TRISO particles exposed to high temperatures (T>1,200°C) and high partial pressures of steam (pH_2O>20%) and determined that under the testing conditions, the fracture strength of the SiC decreases [11, 44]. Despite the decrease in fracture strength due to thinning of the oxidized SiC layer, the TRISO particle is predicted to still withstand the pressures due to internal fission gas pressure until the SiC layer reaches a thickness of 20 μm [11]. The oxidized SiC layer in this study is expected to maintain its integrity and ability to retain fission products and withstand internal pressures during operation. Following that the dominant oxidation regime was passive, the amount of SiO_2 growth shows limited SiC consumption that not enough to cause the SiC layer thickness to reach the 20 μm limit [11].

4.2. Recession determination methods

Two methods were used to determine the resulting SiC layer thickness following oxidation and the results are shown in Table 3. Discrepancies resulted from both techniques, and overall, there is no agreement on the magnitude of SiC recession as the measurements are within the error of both techniques. The lack of agreement displays the need for research that captures micro- to nano-scale changes under extreme conditions while providing statistically relevant and high-fidelity data. The following sections discuss the limitations of both techniques.

4.2.1. Electron microscopy based methods

Two particles from each condition were selected to be cross-sectioned and imaged. Micrographs were calibrated using the scale bar provided during imaging to provide the μm/pixel number. An average of 10 radial measurements at various locations were taken for each particle's SiC cross-section. This measurement was performed on both the as-received and oxidized particles for comparison with two particles analyzed for each condition. The averages of the as-received and each oxidation condition were then subtracted from each other to determine the amount of recession that occurred for the sample set. The measured thickness is 2.6 μm larger than that reported by the ORNL, (33.6 μm ±0.8μm) for these particles [34]. While it is closer in agreement with a recent study (SiC layer reported to be 35.0 μm) that also tested AGRBW-4A2 ZrO_2 kernel particles [11], the lack of midplane corrections in both this study and in [11] bias the measured value higher and the limited number of particles analyzed fail to capture the statistical distribution of SiC layer thickness. When measuring TRISO layer thickness using microscopy methods, particles must either be polished very close to the midplane or apply a geometric midplane correction. In addition, a significant number of particles (100's) must be measured to accurately capture the statistical distribution of variable parameters. While ion milling and subsequent microscopy are sensitive to sub-micron microstructural changes, the variation from particle to particle increases the uncertainty in the measurement. This variation in measurements highlights the need for appropriate sampling to improve the fidelity of certain analysis approaches, as measurable oxide growth is observed, however the SiC recession is within the propagated uncertainty of these techniques. The anticipated uncertainty is acknowledged and consistent approaches to measure SiC thickness were applied for the SiC recession analysis presented in Table 3.

4.2.2. Shadow imaging via optical microscopy and statistical analysis

Shadow imaging has been shown to be accurate in its measurement of the TRISO particle diameters and capable of measuring particle size distribution when sample sets are at least 80 particles in size [34]. The amount of particles used in this investigation, 20–50 oxidized particles, is lower than standard shadow imaging processes applied at ORNL, resulting in greater uncertainty [34]. Using the stitched optical micrographs described in section 2.5, the images were processed using the algorithm described in Price et al. [48, 49]. The algorithm identifies the edges using Sobel edge-detection and takes 360 measurements around the circumference of the particles. Outlier points are identified and discarded based on comparison with neighbors and statistics of each condition. The average of the 360 measurements for each particle within individual each oxidation condition is reported. The mean kernel and IPyC contributions to the diameter along with their standard deviation values were obtained from the fabrication report [34], and SiO_2 thickness measurements from the FIB cross sections were subtracted out. The remaining value would be the SiC layer thickness for that condition. Automated image processing software is used to identify each particle and measure its boundary, allowing for the calculation of mean diameter and other attributes (e.g., aspect ratio or local curvatures) for each particle. When this approach is used on a mount with many particles, it produces a statistical distribution of particle diameters.

The challenges of using this technique for determination of the SiC layer thickness is that the direct measurement is of the particle diameter and the SiC layer thickness is thereby inferred, resulting in statistical uncertainty introduced by subtracting the mean kernel and internal layer thicknesses, each of which have a given mean and standard deviation as reported by the Advance gas reactor (AGR) program [34]. Additionally, a limited number of particles (20-50) are available for measurement to form a robust statistical distribution. Using this technique in the present study,

the mean SiC layer thickness was determined to be 27.1 μm (SD=9.1 μm) with a standard error of 1.8 and a kernel diameter of 672 μm (SD=9.4 μm) using as-received particles. Using uncertainty propagation and the SD values for the kernel and IPyC from the fabrication report [34], particle statistics are the main factors that contribute to the observed uncertainty. If a greater particle sample set was used, then it is expected that the SD, and associated uncertainty, which is currently within 2 SD of the AGR report, would decrease and align more with the reported values of both SiC layer thickness and its SD in reference [34]. Although the value will be closer, it will not match the reported value in the AGR report [34]; this measurement technique does propagate the uncertainty from the kernel and IPyC. The SiC thickness reported in [34] is a direct measurement that does not propagate that same uncertainty.

A likely optimal approach to directly measure SiC recession would be to leverage the layer thickness measurement approach described in Hunn, Byun, and Miller [34] on a statistically significant population of particles. This approach used a combination of cross-sectioning and optical imaging to determine the SiC layer thickness [50]. A grid of 80 samples was ground down a set known distance (200 μm) to approximately midplane and then polished for imaging. This materialographic method allowed the samples to remain planar and limited artifacts from sample preparation impacted the measurement. Using an automated optical system, serial imaging of the cross-sections was performed, and in-house software identified 720 points on each interface while applying a geometrical correction to account for the samples being approximately midplane [48, 49]. The image analysis would then produce the mean layer thickness and kernel radius as the measurement average and SD for each particle. The direct measurement isolates the thickness variation of the SiC layer only in the statistical population and therefore does not propagate uncertainty from inner layers (e.g. IPyC and kernel in the particles explored here). The aforementioned method would likely present SD on the order of 0.8 μm based on 720 measured thickness values from each of the 80 particles [34] allowing for recession greater than 1.6 μm to be measured. Alternatively, recession could be measured by less sensitive techniques if conditions exploring significant layer recession greater than the SD associated with the previously described approaches were pursued.

	Microscopic Measurements		**Shadow Imaging Analysis**			
Condition	**Average SiC recession (μm)**	**Standard deviation for SiC recession (μm)**	**Particle diameters (μm)**	**Standard deviation for particle diameter (μm)**	**SiC recession from shadow imaging (μm)**	**Standard error for particle diameter (μm)**
5% H_2O+1% CO	0.87	0.64	669	9.1	1.6	2.1
5% H_2O+0.1% CO	0.84	1.2	673	9.4	0.54	1.3
5% H_2O	0.88	0.68	674	9.7	-0.30	1.2
9% H_2O+1% CO	0.42	1.3	672	8.1	0.86	1.3
9% H_2O+0.1%CO	0.25	1.1	673	9.7	0.64	1.4
9% H_2O	0.83	0.51	678	6.8	-1.5	1.8
21%H_2O+1% CO	1.0	0.87	672	7.4	1.4	1.2

21%H_2O+0.1%CO	1.2	0.92	675	7.6	0.48	1.1
21% H_2O	1.3	0.44	668	9.1	2.6	1.0

Table 3-Summary of measurements on SiC recession had occurred utilizing both microscopic and shadow imaging analysis.

5. Conclusion

The complex behavior of the SiC layer under mixed gas atmospheres at T = 1,200°C was observed, and the investigation concludes that the SiC underwent predominantly passive oxidation with potential SiC recession. The TRISO particle oxidation in varying partial pressures of steam and CO formed a crystalline SiO_2 layer that increased in porosity at high pH_2O (pH_2O=21%) conditions. Microstructure analysis determined that exposures with higher CO concentrations paired with low partial pressure of steam (<5%) atmospheres inhibited SiO_2 layer growth, facilitating the potential for active oxidation. SiO_2 growth was most prominent in high pH_2O (>21%) atmospheres suggesting that these conditions exhibited passive oxidation. The study demonstrated how the SiC layer of the TRISO particle in a mixed gas atmosphere forms a crystalline yet porous SiO_2 layer, but the presence of CO, a reducing gas, can limit its growth (<2 μm) and porosity. Under off-normal reactor conditions, the presence of low partial pressures of steam and CO can inhibit the amount of the protective SiO_2 layer. Overall, the SiC layer showed strong oxidation resistance under these accident conditions, limiting SiO_2 growth and maintaining its structural integrity when exposed to various mixed oxidant atmospheres.

This study will be built upon for testing and characterizing SiC-terminated TRISO particles at higher temperatures (T>1,300°C) with similar mixed gas conditions. Testing the particles in mixed gas atmospheres will aid in understanding how steam ingress may cause some of the graphitic components to oxidize, forming a complex atmosphere of steam and volatile oxidation products. Low partial pressures (<10%) of reducing gases, such as CO and H_2, are expected to alter the oxidation response compared to a steam-only condition. As the event continues, the relative abundances of the contaminants are consumed or formed as the scenario progresses. Further investigation into oxidation testing of high-temperature mixed gas atmospheres will better inform on the oxidation performance of the SiC layer.

6.CRediT authorship contribution statement

Katherine I. Montoya: Investigation, Methodology, Writing-Original Draft, Writing-Review and Editing **Brian A. Brigham**: Writing-Original Draft, Writing-Review and Editing **Grant Helmreich:** Formal analysis, Writing-Review and Editing **Jesse W. Werden**: Investigation, Writing-Review and Editing **Tyler J. Gerczak**: Conceptualization, Writing-Review and Editing, **Elizabeth S. Sooby**: Conceptualization, Funding acquisition, Supervision, Writing-Review and Editing

7.Acknowledgements

FIB microscopic measurements were taken in the Low Activation Materials and Development and Analysis facilities at Oak Ridge National Laboratory. Ion milling cross-sectioning was performed at the University of Texas at San Antonio Kleberg Advanced Microscopy Center with the support of Hitachi High-Tech. Materials for this work were provided by the US Department of Energy's

(DOE's) Office of Nuclear Energy Advanced Reactor Technologies as part of the Advanced Gas Reactor Fuel Development and Qualification (AGR) program. This material is based upon work supported by the U.S. Department of Energy, Office of Nuclear Energy AGR Program, ORISE H.E.R.E Program, and Department of Energy Nuclear Energy University Programs. Award Number: DE-NE0008798.

8.References

[1] D.A. Petti, J.T. Maki, J.D. Hunn, P.J. Pappano, C. Barnes, The DOE advanced gas reactor fuel development and qualifications programs, Materials for Nuclear Power 62 (2010).
[2] T. Hicks, Modular HTGR Safety Basis and Approach, INL/EXT-11-22708 Idaho National Laboratory (2011).
[3] P.A. Demkowicz, J.D. Hunn, B. Liu, Coated partical fuel: Historical perspectives and current progress, Journal of Nuclear Materials 515 (2019) 434-450.
[4] J. Wen, J.D. Hales, S.B. W., B.P. Collin, A.E. Slaughter, S. Novascone, A. Toptan, K. Gamble, R. Gardner, TRISO particle fuel performance and failure analysis with BISON, Journal of Nuclear Materials 548 (2021).
[5] W.F. Skerjanc, J.T. Maki, B.P. Collin, D.A. Petti, Evaluation of design parameters for TRISO-coated fuel particles to establish manufacturing critical limits using PARFUME, Journal of Nuclear Materials 469 (2016) 99-105.
[6] G.K. Miller, D.A. Petti, J.T. Maki, D.L. Knudson, W.F. Skerjanc, PARFUME Theory and Model Basis Report, NL/EXT-08-14497 (2018).
[7] K. Minato, T. Ogawa, K. Fukuda, M. Shimizu, T. Yoshinobu, I. Takahashi, Fission Product behavior in TRISO-coated UO2 Fuel Particles, Journal Of nuclear Materials 208 (1994) 266-281.
[8] J.D. Hunn, C.A. Baldwin, F.C. Montgomery, T.J. Gerczak, R.N. Morris, G.W. Helmreich, P.A. Demkowicz, J.M. Harp, J. Stempien, Inital examination of fuel comapcts and TRISO particles from the US ARG-2 irradiation test, Nuclear Engineering and Design 329 (2018) 89-101.
[9] J.D. Hunn, C.A. Baldwin, T.J. Gerczak, F.C. Montgomery, R.N. Morris, C.M. Silva, P.A. Demkowicz, J.M. Harp, S.A. Ploger, Detection and analysis of particles with failed SiC in AGR-1 fuel compacts, Nuclear Engineering and design 306 (2016).
[10] G.K. Miller, D.A. Petti, J.T. Maki, D.L. Knudson, An evaulation of the effects of SiC layer thinning on failure of TRISO coated fuel particles, Journal of Nuclear Materials (2006).
[11] Y. Cho, K. Lu, Water vapor oxidation of SiC layer in surrogate TRISO fuel particles, Composites Part B 215 (2021).
[12] J. Wolters, R. Bongartz, R. Moormann, The significance of water ingress accidents in small HTRs, Nuclear Engineering and Design 109(1-2) (1988) 289-294.
[13] Preliminary Safety Information Document for the Standard MHTGR, HTGR-86-024 1 (1986).
[14] T.J. Gerczak, C.I. Contescu, Y.H. Lee, R.W. Mee, A. Schumacher, J. Stempien, M.P. Trammell, Oxidation of Matrix Material in Helium Varied Moisture Content, ORNL/TM-2019/1341 (2019).
[15] Z. Yanhua, S. Lei, Y. Wang, Water-ingress analysis for the 200 MWe pebble-bed modular high temperature gas-cooled reactor, Nuclear Engineering and Design 240(10) (2010) 3095-3107.
[16] G.H. Lohnert, The consequences of water ingress into the primary circuit of an HTR-Modeule- From design basis accident to hpothetical postulates, Nuclear Engineering and Design 134(2-3) (1992) 159-176.

[17] M.B. Richards, D.L. Hanson, R.F. Turner, Fisson-Gas Release During Hydrolysis of Exposed Fuel Kernel, Specialists Meeting on Behavior of Gas-Cooled Reactor Fuel Under Accident Conditions, International Atomic Energy Agency, 1991.
[18] B.A. Brigham, K.I. Montoya, T.J. Gerczak, E.S. Sooby, Determination of oxidation rates and volatile oxidation products for HTGR graphite matrix material exposed to steam atmospheres, Journal of Nuclear Materials 557 (2021) 153256.
[19] A. Roine, HSC Chemistry Software, in: Outotec (Ed.) Pori Software, 2018.
[20] E.J. Opila, D. Fox, G.M. Jacobsen, Mass Spectrometric identification of Si-O-H(g) Species from the Reaction of Silica with water vapor at atmospheric Pressure, J. Am. Ceram. Soc. 80 (1997).
[21] E.J. Opila, N.S. Jacobson, SiO(g) formation from SiC in mixed oxidizing-reducing gases, Oxidation of Metals 44(5) (1995) 527-544.
[22] N.S. Jacobson, E.J. Opila, D. Myers, E.H. Copland, Thermodynamics of gas phase species in the Si-O-H system, J. Chem. Thermodynamics 37 (2005).
[23] V. Presser, K.G. Nickel, Silica on Silicon Carbide, Critical Reviews in Solid State and Materials Sciences 33 (2008) 1-99.
[24] M. Balat, R. Bejoan, G. Pichelin, D. Rochman, High temperature oxidation of sintered silicon carbide under pure CO2 at low pressure: active-passive transition, Applied Surface Science (1998) 115-123.
[25] V. Avincola, D. Cupid, H.J. Seifert, Thermodynamic modeling of the silica volatilization in steam related to silicon carbide oxidation, Journal of the European Ceramic Society 35 (2015) 3809-3818.
[26] E.J. Opila, N.S. Jacobson, D.L. Myers, E.H. Copland, Predicting oxide stability in high-temperature water vapor, Jom 58(1) (2006) 22-28.
[27] E. Opila, Variation of the Oxidation Rate of Silicon Carbide with Water-Vapor Pressure, Journal of American Ceramic Society 82(3) (1999) 625-36.
[28] E.J. Opila, N.S. Jacobson, SiO(g) Formation from SiC in Mixed Oxidizing-Reducing Gases, Oxidation of Metals 44(5/6) (1995) 527-544.
[29] E.J. Opila, SiC Recession caused by SiO2 scale volatility under combustion conditions:II, thermodynamics and gaseous-diffusion model, Journal of American Ceramic Society 82(7) (1999).
[30] R.C. Robinson, SiC recession caused by SiO2 volatility under combustion conditions: I, Experimental Results and Empirical Model, J. Am. Ceram. Soc. 82(7) (1999) 1817-25.
[31] E.J. Opila, J.L. Smialek, R.C. Robinson, D. Fox, N.S. Jacobson, SiC Recession Caused by SiO2 Scale Volatility under Combustion Conditions: II, Thermodynamics and Gaseous-Diffusion Model, Journal of the American Ceramic Society 82(7) (2004) 1826-1834.
[32] I.J. van Rooyen, D.E. Janney, B.D. Miller, P.A. Demkowicz, J. Riesterer, Electron microscopic evaluation and fission product identification of irradiated TRISO coated particles from the AGR-1 experiment: A preliminary review, Nuclear Engineering and Design 271 (2014) 114-122.
[33] B.A. Brigham, K.I. Montoya, T.J. Gerczak, E.S. Sooby, Analysis of Graphite Matrix Kinetics and Burnoff Products under Off-Normal High-Temperature Gas-Cooled Reactors Conditions, Transaction of American Nuclear Society 122 (2020) 349 to 352.
[34] J.D. Hunn, T.-S. Byun, J. Miller, Fabrication and characterization of Sixteen SiC Variants Deposited on the same IPyC substrate for fracture strength, ORNL/TM-2009/324 (2009).

[35] P. Hosemann, J.N. Martos, D. Frazer, G. Vasudevamurthy, T.-S. Byun, J.D. Hunn, B.C. Jolly, K.A. Terrani, M. Okunsiewski, Mechanical characteristics of SiC coating layer in TRISO fuel particles, Journal of Nuclear Materials 442(1-3) (2013) 133-142.
[36] T.J. Gerczak, J.D. Hunn, R.A. Lowden, T.R. Allen, SiC layer microstructure in AGR-1 and AGR-2 TRISO fuel particles and the influence of its variation on the effective diffusion of key fission products, Journal of Nuclear Materials 480 (2016) 257-270.
[37] A. Bratten, V. Jalan, T.J. Gerczak, H. Wen, Oxide evolution on the SiC layer of TRISO particles during extended air oxidation, Journal of Nuclear Materials 558 (2022).
[38] C.A. Schneirder, W.S. Rasband, K.W. Eliceiri, NIH Image to ImageJ: 25 years of image analysis, Nature Methods 9(7) (2012) 671-675.
[39] A.K. Kercher, J.D. Hunn, J.R. Price, P.J. Pappano, Automated optical microscopy of coated particle fuel, Journal of Nuclear Materials 380 (2008) 74-84.
[40] K.A. Terrani, C.M. Silva, High temperature steam oxidation of SiC coating layer of TRISO fuel particles, Journal of Nuclear Materials 460 (2015) 160-165.
[41] K.A. Terrani, B.A. Pint, C.M. Parish, C.M. Silva, L.L. Snead, Y. Katoh, Silicon Carbide Oxidation in Steam up to 2 MPa, American Ceramic Society 97(8) (2014) 2331-2352.
[42] L. Snead, T. Nozawa, Y. Katoh, T.-S. Byun, S. Kondo, D.A. Petti, Handbook of SiC properties for fuel performance modeling, Journal of Nuclear Materials 371(1-3) (2007) 329-377.
[43] I. Swainson, M. Dove, On the Thermal Expansion of B-Cristobalite, Phys. Chem. Miner 22 (1995).
[44] F. Cao, W. Hao, F. Guo, X. Wang, X. Zhao, N. Rohbeck, P. Xiao, Effects of water vapor on the oxidation and the fracture strength of SiC layer in TRISO particles, Journal of the American Ceramic Society 100(5) (2017).
[45] D.A. Petti, P.A. Demkowicz, J.T. Maki, R.R. Hobbins, 3.07 - TRISO-Coated Particle Fuel Performance, in: R.J.M. Konings (Ed.), Comprehensive Nuclear Materials, Elsevier, Oxford, 2012, pp. 151-213.
[46] R. Liu, B. Liu, K. Zhang, M. Liu, Y. Shao, C. Tang, High temperature oxidation behavior of SiC coating in TRISO coated particles, Journal of Nuclear Materials 453(1-3) (2014) 107-114.
[47] E.J. Opila, Influence of alumina reaction tube impurites on the oxidation of chemically-vapor deposited silicon carbide, Journal of the American Ceramic Society 78(4) (1995) 1107-1110.
[48] J.R. Price, J.D. Hunn, Optical Inspection of coated-particle nuclear fuel, Proceedings of SPIE 5303 (2004).
[49] J.R. Price, D. Aykac, J.D. Hunn, A.K. Kercher, R.N. Morris, New developments in image-based characterization of coated particle nuclear fuel, Proceedings of SPIE 6070 (2006).
[50] J.R. Price, D. Aykac, J.D. Hunn, A.K. Kercher, Automatic characterization of cross-sectional coated particle nuclear fuel using greedy coupled Bayesian snakes, Machine Vision Applications in Industrial Inspection XV, SPIE, 2007, pp. 9-18.